J. Marine. Sci. Appl. (2010) 9: 63-68
DOI: 10.1007/s11804-010-8090-4

Simulation of Cavitating Flow around a 2-D Hydrofoil

Sheng Huang, Miao He*, Chao Wang and Xin Chang

College of Shipbuilding Engineering University, Harbin Engineering University, Harbin 150001, China

Abstract: In order to predict the effects of cavitation on a hydrofoil, the state equations of the cavitation model were combined with a linear viscous turbulent method for mixed fluids in the computational fluid dynamics (CFD) software FLUENT to simulate steady cavitating flow. At a fixed attack angle, pressure distributions and volume fractions of vapor at different cavitation numbers were simulated, and the results on foil sections agreed well with experimental data. In addition, at the various cavitation numbers, the vapor fractions at different attack angles were also predicted. The vapor region moved towards the front of the airfoil and the length of the cavity grew with increased attack angle. The results show that this method of applying FLUENT to simulate cavitation is reliable.
Keywords: 2-D hydrofoil; cavitation model; cavitation flow
Article ID: 1671-9433(2010)01-0063-06

1 Introduction

Cavitation is a phenomenon that plays a major role in surface sea-going vessel design and operation, as well as in hydraulic equipment. Propellers, hydrofoil ships, hydraulic turbines and pumps may suffer from its consequences in many ways. Cavitation can lead to fatal failures of hydraulic machinery and hydraulic structures. Therefore, it has to be avoided or at least controlled. This demands that cavitation inception has to be predicted by means of experiments or numerical investigations during the design phase. Due to the rapid development and broader application of powerful computers and the ability to save costs and time in comparison with experiments, numerical methods have become increasingly popular in recent years.

A number of researchers have been investigating cavitation numerically. Kubota *et al*. (1992) assumed that the fluid initially contains uniformly distributed small gas bubbles that will behave as described by the Rayleigh-Plesset equation in a changing pressure field. Song *et al*. (1997) assumed that, for a natural cavitation, the liquid and gas phases are represented by a single continuous equation of state. Kunz *et al*. (2000) developed a multiphase flow model in which the density of each component is assumed to be a constant. Singhal *et al*. (2001) developed the full cavitation model which assumes the working fluid to be a mixture of liquid, liquid vapor and non-condensable gas (NCG).

In this work, the full cavitation model is adopted. A user-define function is added into the software FLUENT. Pressure coefficients are presented for flows over NACA66 2-D hydrofoils and the computed results are compared with experimental data. Volume fractions of vapor on NACA66 hydrofoils are also predicted.

2 Governing equations and cavitation model

2.1 Governing equations

The cavitaion model implemented is the multiphase mixture model. With proper cavitation model, it can simulate the process of vapor generation and condensation. It assumes that, in a flowing fluid, there is no velocity slip between the fluid and bubbles, and cavitating flow works at constant temperature. The steady state governing equations are given by:

$$\frac{\partial y_l \rho_m u_j}{\partial x_l} = S_l \tag{1}$$

$$\frac{\partial y_v \rho_m u_j}{\partial x_j} = S_v \tag{2}$$

$$\frac{\partial y_g \rho_m u_j}{\partial x_j} = 0 \tag{3}$$

$$\frac{\partial \rho_m u_j u_i}{\partial x_j} = \frac{\partial P}{\partial x_i} + \frac{\partial \tau_{ij}}{\partial x_j} + \rho_m g_i \tag{4}$$

The source terms S_l and S_v denoting vapor generation and condensation rates are calculated as follows

$$S_l = \left(\overline{m_l} + \overline{m_v}\right), \quad S_v = -\left(\overline{m_l} + \overline{m_v}\right)$$

The mixture density of liquid, vapor and NCG is modified as:

$$\rho_m = \alpha_l \rho_l + \alpha_v \rho_v + \alpha_g \rho_g \tag{5}$$

where ρ_l, ρ_v and ρ_g are densities of the liquid, the vapor and NCG, respectively, α_l, α_v and α_g are volume

Received date: 2008-12-23.
***Corresponding author Email:** miaomiao591213@yahoo.com.cn

fractions respectively, and $y_i=\dfrac{\alpha_i\rho_i}{\rho_m}$ represents mass fractions of species *i*.

2.2 Cavitation model

Based on different definitions of density of a single phase, the cavitation models could be categorized into two general classes: the first employs state equations while the second employs transport equations. The full cavitation model focusing on the transport equations is adopted here.

$$\begin{cases} m_l=-C_e\dfrac{\sqrt{k}}{\sigma}\rho_l\rho_v\left(\dfrac{2}{3}\dfrac{p_v-p}{\rho_l}\right)^{1/2}y_l & \text{if } p<p_v \\ m_v=C_c\dfrac{\sqrt{k}}{\sigma}\rho_l\rho_l\left(\dfrac{2}{3}\dfrac{p-p_v}{\rho_l}\right)^{1/2}y_v & \text{if } p>p_v \end{cases} \tag{6}$$

where, the recommended values of the empirical constants C_e and C_c are 0.02 and 0.01, respectively.

3 Turbulence models and near-wall fuctions

3.1 Turbulence models

By analysing all turbulence models in FLUENT, standard $k-\varepsilon$ model, RNG $k-\varepsilon$ model and RSM model are picked out by introduction. They will be compared and one of them will be chosen for further study.

3.1.1 Standard $k-\varepsilon$ turbulence model

The standard $k-\varepsilon$ model (Launder and Spalding, 1972) is a semi-empirical model based on model transport equations for the turbulence kinetic energy(*k*) and its dissipation rate(ε). The model transport equation for *k* is derived from the exact equation, while the model transport equation for ε was obtained using physical reasoning and bears little resemblance to its mathematically exact counterpart .It assumes that the flow field is onflow, and the viscosity between numerator is ignored, so the standard $k-\varepsilon$ model is availability only in the onflow.

The transport equations of the standared $k-\varepsilon$ model are given by

$$\rho\frac{\mathrm{D}k}{\mathrm{D}t}=\frac{\partial}{\partial x_i}\left[\left(\mu+\frac{\mu_t}{\sigma_k}\right)\frac{\partial k}{\partial x_i}\right]+G_k+G_b-\rho\varepsilon \tag{7}$$

$$\rho\frac{\mathrm{D}\varepsilon}{\mathrm{D}t}=\frac{\partial}{\partial x_i}\left[\left(\mu+\frac{\mu_t}{\sigma_k}\right)\frac{\partial \varepsilon}{\partial x_i}\right]+C_{1\varepsilon}\frac{\varepsilon}{k}(G_k+C_{3\varepsilon}G_b)-C_{2\varepsilon}\rho\frac{\varepsilon^2}{k} \tag{8}$$

where, G_k represents onflow kinetic energy arosed by average speed grads, and G_b represents onflow kinetic energy arosed by flotage effect. The viscosity coefficient of the onflow is $\mu_t=\rho C_\mu\dfrac{k^2}{\varepsilon}$. $C_{1\varepsilon}=1.44$, $C_{2\varepsilon}=1.92$, $C_\mu=0.09$, $\sigma_k=1.0$, $\sigma_\varepsilon=1.3$.

3.1.2 RNG $k-\varepsilon$ model

The RNG $k-\varepsilon$ model (Choudhury, 1993) was derived using a rigorous statistical technique (called renormalization group theory). It is similar in form to the standard $k-\varepsilon$ model, but it has an additional term in its ε equation that significantly improves the accuracy for rapidly strained flows. The transport equations of the RNG $k-\varepsilon$ model are given by:

$$\rho\frac{\mathrm{D}k}{\mathrm{D}t}=\frac{\partial}{\partial x_j}\left[\alpha_k\mu_{eff}\frac{\partial k}{\partial x_j}\right]+G_k+G_b-\rho\varepsilon \tag{9}$$

$$\rho\frac{\mathrm{D}\varepsilon}{\mathrm{D}t}=\frac{\partial}{\partial}\left[\alpha_\varepsilon\mu_{eff}\frac{\partial \varepsilon}{\partial x_j}\right]+C_{1\varepsilon}\frac{\varepsilon}{k}(G_k+C_{3\varepsilon}G_b)-C_{2\varepsilon}\rho\frac{\varepsilon^2}{k}-R_\varepsilon \tag{10}$$

where, $C_{1\varepsilon}=1.42$, $C_{2\varepsilon}=1.68$, $C_\eta=\dfrac{\eta(1-\eta/\eta_0)}{1+\beta\eta^3}$, $\eta=Sk/\varepsilon$, $S=\sqrt{2\overline{S_{ij}S_{ij}}}$, $\eta_0=4.28$, $\beta=0.015$, $C_\mu=0.085$, $C_{3\varepsilon}=[-1+2C_{1\varepsilon}-3m_1(n-1)+(-1)^\delta\sqrt{6}C_\mu C_\eta\eta]/3$.

3.1.3 RSM model

The basal Renault stress model (RSM) (Launder *et al*., 1975) is a linearity RSM where linearity algebra equation is used to simulate stress variety item and scalar quantity dissipation equation is used to simulate dissipation item. Equations in the RSM model are given by:

$$\frac{\partial}{\partial t}(\rho\overline{u_iu_j})+\frac{\partial}{\partial x_k}(\rho U_k\overline{u_iu_j})=D_{ij}+P_{ij}+\Phi_{ij}-\varepsilon_{ij} \tag{11}$$

where, D_{ij} is the diffuse item, P_{ij} the produce item, Φ_{ij} the stress variety item, and ε_{ij} the dissipation item,which are given as below:

$$D_{ij}=\frac{\partial}{\partial x_k}\left(\frac{\mu_t}{\sigma_k}\frac{\partial\overline{u'_iu'_j}}{\partial x_k}\right)$$

$$P_{ij}=-\left(\overline{u'_iu'_k}\frac{\partial U_j}{\partial x_k}+\overline{u'_ju'_k}\frac{\partial U_i}{\partial x_k}\right)$$

$$\Phi_{ij}=-C_1\varepsilon\alpha_{ij}+C_2\varepsilon\left(\alpha_{ik}\alpha_{kj}-\frac{1}{3}\alpha_{kl}\alpha_{kl}\delta_{ij}\right)+C_3kS_{ij}+C_4k\left(\alpha_{ik}S_{jk}+\alpha_{jk}S_{ik}-\frac{2}{3}\alpha_{kl}\alpha_{kl}\delta_{ij}\right)+C_5(\alpha_{ik}W_{jk}+\alpha_{jk}W_{ik})$$

Comparing with the double equation $k-\varepsilon$ model, the RSM model doesn't need any transportion equation to sulotion.

3.2 Near-wall functions

For cavitation happens near the wall, near-wall treatments

influence precision of cavitation flow simulation. Near-wall treatments contained in the FLUENT are: standard wall function, non-equilibrium wall function and enhanced wall function.

3.2.1 Standard wall function

The standard wall functions in FLUENT are based on the proposal of Launder and Spalding (1974), and have been most widely used for industrial flows.The equations are given by:

$$\begin{cases} U^+ = \dfrac{1}{k}\ln\left(Ey^+\right) & y^+ > 11.225 \\ U^+ = y^+ & y^+ < 11.225 \end{cases} \tag{12}$$

where, $k = 0.42, E = 9.8$, $U^+ = \dfrac{U_P c_\mu^{1/4} k_P^{1/2}}{\tau w/\rho}$, $y^+ = \dfrac{\rho c_\mu^{1/4} \kappa_P^{1/2} y^P}{\mu}$.

3.2.2 Non-equilibrium wall function

Non-equilibrium wall function adopte stress grads on basis of standard wall function method,the equations are given below:

$$\frac{\tilde{U} c_\mu^{1/4} k^{1/2}}{\tau w/\rho} = \frac{1}{\kappa}\ln\left(E\frac{\rho c_\mu^{1/4} k^{1/2} y}{\mu}\right) \tag{13}$$

where,

$$\tilde{U} = U - \frac{1}{2}\frac{\mathrm{d}p}{\mathrm{d}x}\left[\frac{y_v}{\rho\kappa\sqrt{k}}\ln\left(\frac{y}{y_v}\right) + \frac{y - y_v}{\rho\kappa\sqrt{k}} + \frac{y_v^2}{\mu}\right],\ y_v = \frac{\mu y_v^*}{\rho c_\mu^{1/4}\kappa_p^{1/2}},$$

$y^* = 11.225$.

3.2.3 Enhanced wall function

Enhanced wall function formulates the law-of-the wall as a single wall law for the entire wall region. It blends linear (laminar) and logarithmic (turbulent) laws-of-the-wall using a function suggested by Jongen (1992):

$$u^+ = e^{\Gamma} u_{lam}^+ + e^{\frac{1}{\Gamma}} u_{turb}^+ \tag{14}$$

where, $\Gamma = \dfrac{a\left(y^+\right)^4}{1 + by^+}$, $a = 0.01c$, $b = 5/c$

4 Grid generation and boundary conditions

4.1 Model geometry and grid generation

A NACA66 (mod) hydrofoil section with camber ratio of 0.02, mean line length of 0.8 and thickness of 0.09 was used. A 2-D working section of the hydrofoil surface was mounted in a water tunnel.

It is known that one of the most significant parameters in numerical flow simulations is the quality of mesh. This affects directly the accuracy of solution and the required number of iterations (CPU time). For this purpose, the computational domain modeling flow over the hydrofoil contains 30 000 structured meshes. Meshes near the airfoil are denser, as shown in Fig.1

4.2 Boundary conditions

The nature of the equations dictates the application of proper boundary conditions on all boundaries. We apply the no-slip, no flux boundary condition to the velocity on the surface of the airfoil and constant velocity on boundary I (Fig.1). Pressure outlet condition is applied on boundary II. A second-order upwind scheme is used to discrete the convective fluxes. The nature of the equations dictates the application of proper boundary conditions on all boundaries. The working fluid is water at 300 K, with liquid and vapor densities of 1 000 and 0.025 58 kg/m^3, saturation pressure of 3 540 Pa and surface tension of 0.071 7 N/m.

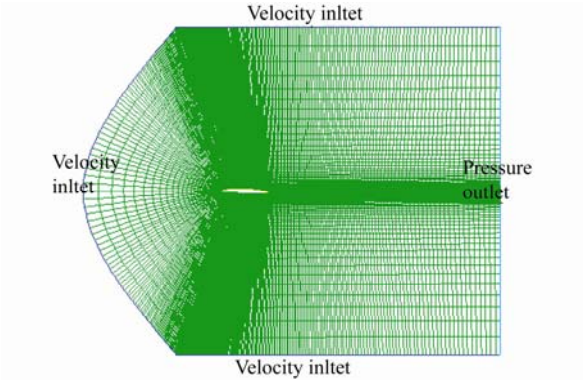

(a) Boundary conditions

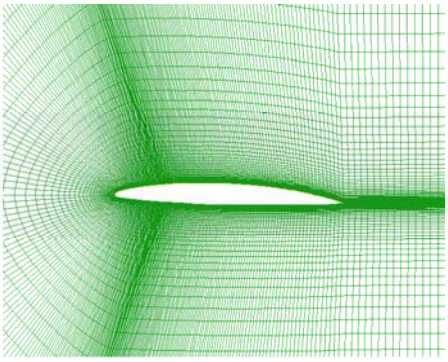

(b) Mesh details

Fig.1 Computation domain and grid, and grid distribution near the hydrofoil for α =4º

5 Simulation results

Static pressures on hydrofoil surface were measured at different angles of attack and σ values. Simulations were performed at $Re = 2\times10^6$. The non-dimensional parameters of interest were:

$$Re = \frac{\rho_l U_\infty C}{\mu_l},\quad \sigma = \frac{P_\infty - P_v}{\frac{1}{2}\rho_l U_\infty^2},\quad C_p = \frac{P - P_\infty}{\frac{1}{2}\rho_l U_\infty^2}.$$

5.1 Comparison of different turbulence models

In order to choose a appropriate turbulence model for further study, all three turbulence models mentioned above are compared before prediction. The comparison is carried out using standard near-wall function and the cavity number is

0.84. The pressure coefficient distribution at different turbulence models are given by Fig.2.

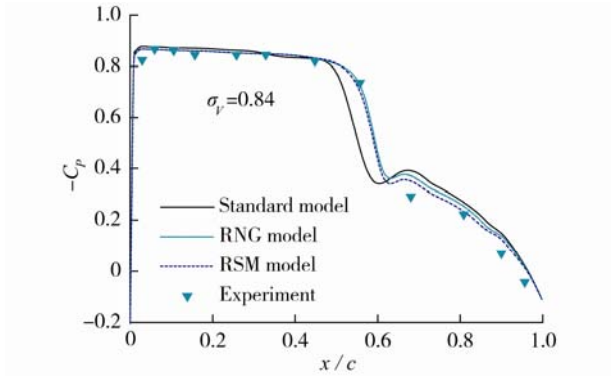

Fig.2 Pressure variation on the suction side by different turbulence models

As shown in Fig.2, calculation results of the RNG model and the RSM model are more consistent, and agree well with experimental data. After considering computing time and results, the RNG model is chosen here for RSM model wastes more time in simulation.

5.2 Comparison of different near-wall fuctions

The near-wall fuctions are also compared in this paper.The comparison is carried out using RNG turbulence model and the cavity number is 0.84. The pressure coefficient distribution curves at different functions are shown in Fig.3.

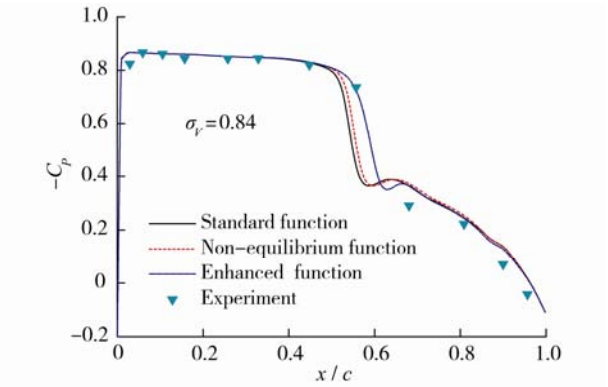

Fig.3 Pressure variation on the suction side by different wall functions

As is shown in Fig.3, calculation results using enhanced near-wall function agree well with experimental data. As a result, the RNG turbulence model combining with enhanced near-wall function is used to predict the effect of cavitation on hydrofoil.

5.3 Various σ values

The first test examines various cavitation numbers at a fixed angle of attack. Choose an attack angle of 4°, while the exit pressure was varied to yield σ values of 1.0, 0.91, 0.84. Calculated C_p values on hydrofoil's top surface are shown in Figs.4~6 together with experimental data, and good agreement is seen. The vapor volume fractions of different σ values are given in Fig.7.

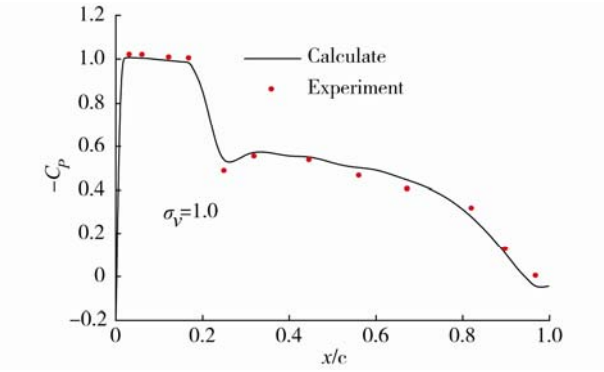

Fig.4 Pressure variation on the suction side of a hydrofoil

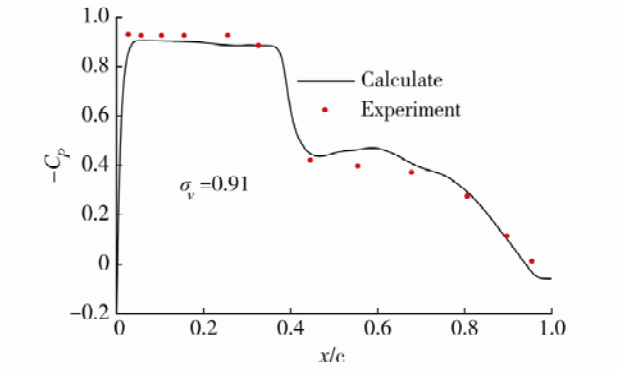

Fig.5 Pressure variation on the suction side of a hydrofoil

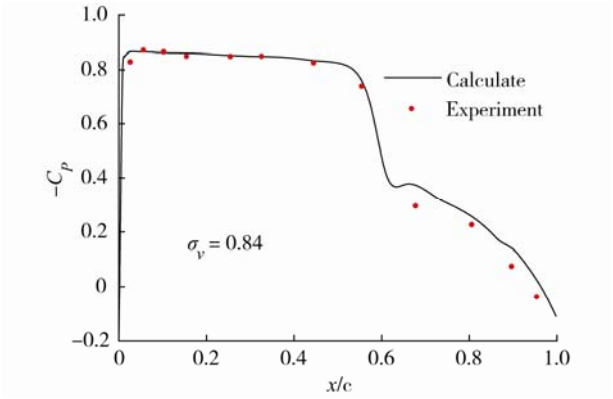

Fig.6 Pressure variation on the suction side of a hydrofoil

As shown in Figs.4~6, it can be seen that the region of the cavity, both length-wise and pressure distribution-wise, is predicted rather well, but as we move downstream along the airfoil surface, there is a growing discrepancy between the experiment and the computations. This phenomenon is even clearer when the σ value is small due to the viscous effects. The peak values of pressure in cavitation regions grow with the decrease of the σ values. In Fig.5, the length of the cavity grows with the decrease of the σ values, as expected.

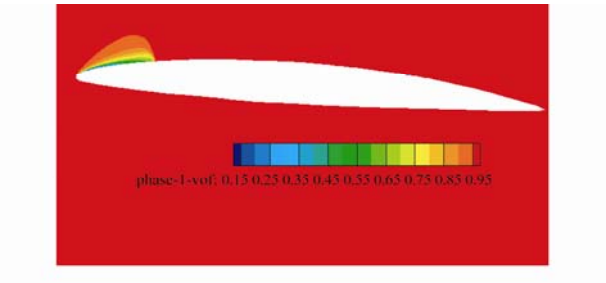

(a) σ =1.0

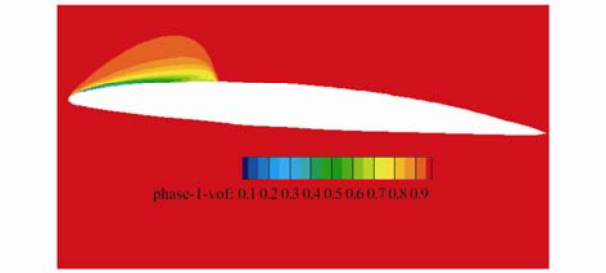

(b) σ =0.91

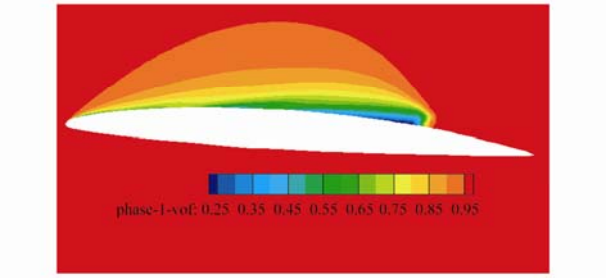

(c) σ =0.84

Fig.7 Computed volume fraction distributions at different cavitation numbers

5.4 Various attack angles

For the second test, we chose σ =0.91 and angles of attack of 0º, 2º, 4º and 6º. The results concerning the vapor volume fraction contours appear in Fig.8. No vapor was observed at angles of attack of 0º and 2º, and the small values of vapor volume fraction appear at the mid-chord region. As the attack angle grows, the vapor region moves to the front of the airfoil. In general, the length of the cavity grows with the increase of the angle of attack, as expected.

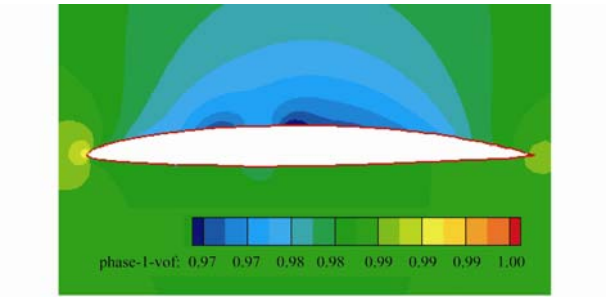

(a) α =0º

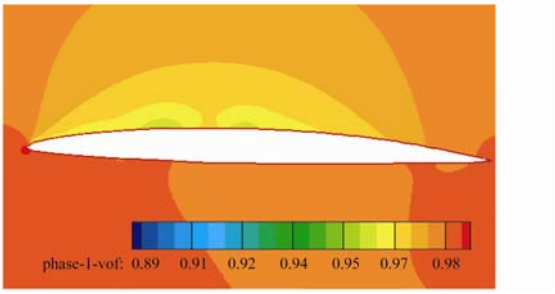

(b) $\alpha = 2°$

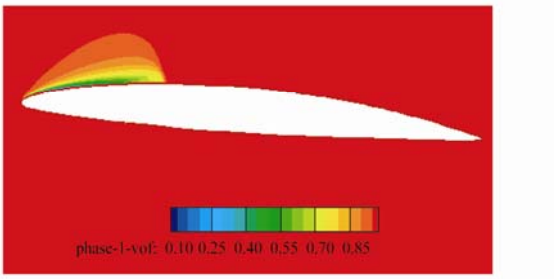

(c) α =4º

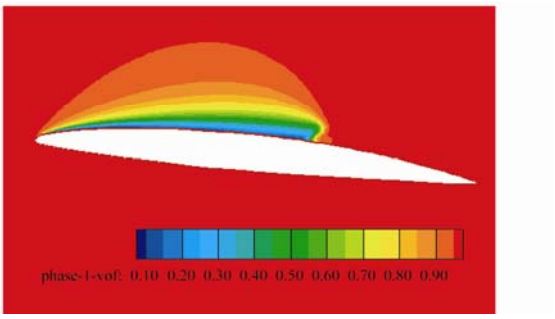

(d) α =6º

Fig.8 Computed volume fraction distributions at different attack angles

6 Summary and conclusions

Steady cavitation flow over a NACA66 (mod) hydrofoil section was predicted using the full cavitation model, focusing on the effects of σ values and attack angles. After analyzing the results of simulation, we can conclude that:

1) Computations for cavitation inception compare satisfactorily with available experiments;

2) At a fixed angle of attack, both the length of the cavity and the peak values of pressure in cavitation regions grow with the decrease of the σ values, while the inception point keeps the same;

3) Discrepancy happened in the close region of a vapor due to viscous effects;

4) At a fixed σ value, the length of the cavity grows with the increase of attack angle, and the inception point moves to upstream.

The cavitation phenomenon is a complex process, involving the interaction of viscous mechanism with it. The further unsteady cavitation predictions are needed for simulation of the formation, growth, shedding and collapse of bubbles.

References

Choudhury D (1993). Introduction to the Renormalization Group Method and Turbulence Modeling. Fluent Inc., Lebanon, USA, Technical Memorandum TM-107.

Jongen T (1992). Simulation and modeling of turbulent incompressible flows. Ph.D. thesis, EPF Lausanne, Lausanne, Switzerland.

Kim SE, Choudhury DE (1995). A near-wall treatment using wall functions sensitized to pressure gradient. *ASME FED Separated and Complex Flows*, **217**, 273-279.

Kubota A, Kato H, Yamaguchi H (1992). A new modeling of cavitating flows: a numerical study of unsteady cavitation on a hydrofoil section. *Journal of fluid Mechanics*, **240**, 59-96.

Kunz RF, Boger DA, Stinebring DR, Chyczewski TS, Lindau JW, Gibeling HJ, Venkateswaran S, Govindan TR (2000). A preconditioned Navier-Stokes method for two-phase flows with application to cavitation prediction. *Computers & Fluids*, **29**(8), 850-872.

Launder BE, Reece GJ, Rodi W (1975). Progress in the development of a Reynolds-Stress turbulence closure. *Journal of fluid Mechanics*, **68**(3), 537-566.

Launder BE, Spalding DB (1972). *Lectures in Mathematical Models of Turbulence*. Academic Press, London.

Launder BE, Spalding DB (1974). The numerical computation of turbulent flows. *Computer Methods in Applied Mechanics and Engineering*, **3**, 269-289.

Singhal AK, Li HY, Athavale MM, Jiang Y (2001). Mathematical basis and validation of the full cavitation model. *ASME-FEDSM'01*, New Orleans.

Song CCS, He J, Zhou F, Wang G (1997). Numerical simulation of caviling and non-cavitating flows over a hydrofoil. University of Minnesota, Minneapolis,USA, SAFL Project Report No. 402.

Sheng Huang was born in 1945. He is a professor at Harbin Engineering University. His current research interests include shipbuilding engineering, marine propulsor and energy-saving.

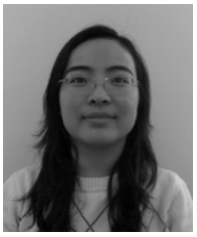

Miao He was born in 1985. She is a doctor at Harbin Engineering University. Her current research interest is ship propulsion.
